Planetary Nebulae: A Universal Toolbox in the Era of Precision Astrophysics
Proceedings IAU Symposium No. 384, 2025
O. De Marco, A. Zijlstra & R. Szczerba, eds.
doi:10.1017/S1743921324000486

GTC Spectroscopic Surveys of Planetary Nebulae in the Milky Way and M31

Xuan Fang[1,2], **Haomiao Huang**[1,3], **Martín A. Guerrero**[4], **Letizia Stanghellini**[5], **Rubén García-Benito**[4], **Ting-Hui Lee**[6] and **Yong Zhang**[7,2]

[1]National Astronomical Observatories, Chinese Academy of Sciences (NAOC), Beijing 100101, China; fangx@nao.cas.cn

[2]Laboratory for Space Research, Faculty of Science, The University of Hong Kong, Hong Kong, China

[3]School of Astronomy and Space Science, University of Chinese Academy of Sciences, Beijing 100049, China

[4]Instituto de Astrofísica de Andalucía, CSIC, Glorieta de la Astronomía s/n, E-18008 Granada, Spain

[5]NSF's NOIRLab, 950 N. Cherry Ave., Tucson, AZ 85719, USA

[6]Department of Physics and Astronomy, Western Kentucky University, Bowling Green, KY 42101, USA

[7]School of Physics and Astronomy, Sun Yat-Sen University, Zhuhai 519082, China

Abstract. We report spectroscopic surveys of planetary nebulae (PNe) in the Milky Way and Andromeda (M31), using the 10.4-m Gran Telescopio Canarias (GTC). The spectra are of high quality and cover the whole optical range, mostly from 3650 Å to beyond 1 μm, enabling detection of nebular emission lines critical for spectral analysis and photoionization modeling. We obtained GTC spectra of 24 compact (angular diameter <5 arcsec) PNe located in the Galactic disk, ∼3–20 kpc from the Galactic centre, and that can be used to constrain stellar evolution models and derive radial abundance gradients of the Milky Way. We have observed 30 PNe in the outer halo of M31 using the GTC. These halo PNe are uniformly metal-rich and probably all evolved from low-mass stars, consistent with the conjecture that they formed from the metal-rich gas in M31 disk but were displaced to their present locations due to galaxy interactions.

Keywords. (ISM:) planetary nebulae: general, stars: evolution, planetary nebulae

1. Introduction

Planetary nebulae (PNe) evolved from low- to intermediate-mass stars (∼1–8 $M_\odot$), which account for an absolute majority of the stellar populations in the universe. PNe are ionized shells of gas ejected episodically by asymptotic giant branch (AGB) stars during the late-stage stellar evolution. Although belonging to the interstellar medium (ISM) and having a very short visible/dynamical age (∼10^4 yr) due to nebular expansion, PNe are a direct link between stellar evolution and the interstellar gas, and can be used to well constrain the theory of AGB nucleosynthesis (e.g. Fang et al. 2018; Henry et al. 2018).

Chemical abundances of PNe, both of α-elements and of N, C and He, can be used to constrain stellar evolutionary models and quantify the contribution of low- to intermediate-mass stars to Galactic chemical enrichment. CNO abundances give a direct indication of whether the AGB stars have gone through hot bottom burning (HBB) and the third dredge-up (Herwig 2005), indicating a more massive progenitor. The α-elements can also be used to constrain Galactic chemical evolution by measuring metallicity gradients in the disk (e.g. Milingo et al. 2010; Stanghellini & Haywood 2010).

Abundances of Galactic PNe have been investigated for decades, but mostly with significant limitations. First, of the current several hundred Galactic PNe with detailed chemical analyses, most are older, extended objects (e.g. Dufour et al. 2015; Henry et al. 2018). Deriving total elemental abundances in extended PNe using small apertures (e.g. narrow slits) involves substantial uncertainties because the ionization is often highly stratified in a PN (Osterbrock & Ferland 2006). It is hard to extrapolate abundances from one part of a PN to the whole nebula. Compact PNe fit into a long slit, so the flux of the entire nebula is measured, and little correction is needed. A second limitation on abundance analyses of Galactic PNe is that results between similar studies by different observations/authors are frequently inconsistent, due to different ionization correction factors (ICFs) adopted. ICFs are used to estimate abundances of ions that are absent in optical spectra (Kingsburgh & Barlow 1994), and work generally well; but since they were never calibrated for extreme metallicity, electron temperature, or ionization levels due to lack of infrared (IR) or UV data at the time, the use of ICFs introduces larger uncertainties in those regimes. Hence, the best way to address this problem is optical spectroscopy in combination with the IR/UV data. That is why we carried out optical spectroscopy of Galactic compact PNe with available *Spitzer* mid-IR and *HST*/STIS UV observations (see Section 2).

The main-sequence progenitors of PNe encompass a wide range of stellar ages, corresponding to a broad range in stellar population. Given their bright, narrow emission lines, PNe are easily detectable in distance galaxies/clusters (e.g. Gerhard et al. 2005, 2007; Longobardi et al. 2018), and are excellent tracers of the chemistry, dynamics and stellar population of host galaxies. The Andromeda Galaxy (M31) is the nearest (785 kpc; McConnachie et al. 2005) large disk system and best candidate for studying galaxy merger and evolution. Numerous large-scale substructures (i.e. stellar streams; e.g. Ibata et al. 2001) as well as inhomogeneity in metallicity have been revealed in M31's extended halo by panoramic surveys such as PAndAS (McConnachie et al. 2009), pointing to a tumultuous merging history of this galaxy.

One long-standing unresolved question is what the origin of M31's stellar substructure is. It has been proposed that the Northern Spur and the Southern Giant Stream, two very prominent substructures, might be connected by a stellar stream (Ibata et al. 2001; Merrett et al. 2003), but this hypothesis needs assessment. Recent hydrodynamical simulations suggests that a single major merger might be responsible for the bulk of the substructures in the M31 halo, including the Southern Giant Stream (Hammer et al. 2018). However, these simulations, including all previous efforts, are still somewhat speculative; accurate observations yet to be used help constrain the modeling. PNe are the only ISM/nebulae that exist in almost every part of a galaxy, from the disk to the bulge as well as the outer halo; the nebular emission lines of a PN can be measured to derive accurate ionic/elemental abundances. PNe thus can be used as a tracer to study the properties of M31 halo substructures. This is the main driving science of our GTC spectroscopy of PNe in M31's halo (see Section 3).

2. Spectroscopic Survey of compact PNe in the Galactic Disk

We carried out deep optical spectroscopy of 24 compact (angular diameter <5 arcsec; Figure 1) PNe in the Galactic disk, using the OSIRIS spectrograph on the 10.4 m Gran Telescopio Canarias (GTC, La Palma). The targets are mostly Northern objects, and

https://doi.org/10.1017/S1743921324000486 Published online by Cambridge University Press

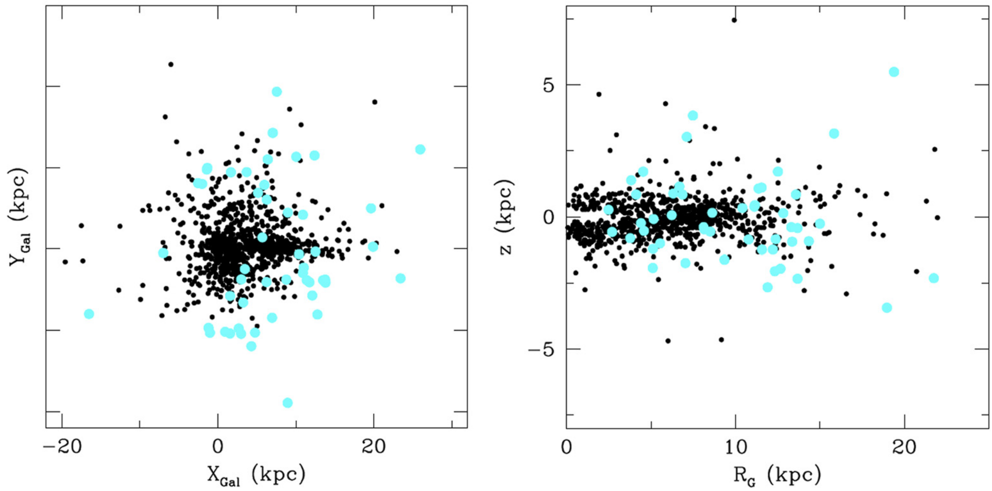

Figure 1. Spatial distribution of compact PNe (large, cyan dots) against the general distribution of Galactic PNe (small, black dots). *Left*: top-view of the Galactic disk. *Right*: galacocentric distance vs. distance from the Galactic plane. Images adopted from Stanghellini, Shaw & Villaver (2016, Figures 8 and 9 therein).

were carefully selected from a well defined sample of 150 compact PNe whose mid-IR spectra were obtained with *Spitzer*/IRS (Stanghellini et al. 2012). They cover an adequate galactocentric range (∼3–20 kpc) so that radial metallicity gradients can be readily available.

The GTC/OSIRIS observations was obtained from June to July in 2016 (GTC program No.: GTC66-16A; PI: X. Fang) in the long-slit spectroscopy mode, with 1 arcsec slit width. The blue and red grisms, R1000B and R1000R, were used, covering spectral ranges ∼3630–7850 Å and ∼5080–10370 Å, respectively. The OSIRIS detector consists of two CCDs with 2048×4096 pixels†. The size of a single pixel is 15 μm, corresponding to angular scale of 0.127 arcsec; the standard observing mode was used where the output images were binned by 2×2. Spectroscopic observations were carried out in the dark moon night with a wonderful seeing of 0.6–0.8 arcsec. During observations, multiplet exposures were made for each PN for purpose of cosmic-ray removal and increasing the signal-to-nose ratio. In total, ∼40 hr observations were completed at GTC for the 24 compact PNe.

Reduction of the GTC OSIRIS spectra generally follows the standard procedure for the long-slit spectra, using IRAF‡. As an example, we present in Figure 2 the final reduced, calibrated and extracted 1D spectrum of one of our targets, PN G068.7+14.8, where C III $\lambda\lambda$4649,5696 and C IV $\lambda\lambda$5801,5811 broad emission lines, probably coming from the PN central star, are well detected. We analyzed the nebular spectra, and carried out photoionization modeling using the Cloudy code (Ferland et al. 1998, 2017) to derived the PN central star properties (e.g. *bottom-right* panel in Figure 2).

Complete analyses of the GTC spectra of all compact PNe targets, in combination with the archival *HST*/STIS UV–optical and *Spitzer* min-IR data, are underway (Fang et al. 2023a, in preparation). The more reliable ICFs of different elements will be derived for

† In 2023, OSIRIS was updated to OSIRIS+, with a new monolithic 4k×4k CCD installed. https://www.gtc.iac.es/instruments/osiris+/osiris+.php

‡ IRAF, the Image Reduction and Analysis Facility, is distributed by the National Optical Astronomy Observatory, which is operated by the Association of Universities for Research in Astronomy under cooperative agreement with the National Science Foundation.

https://doi.org/10.1017/S1743921324000486 Published online by Cambridge University Press

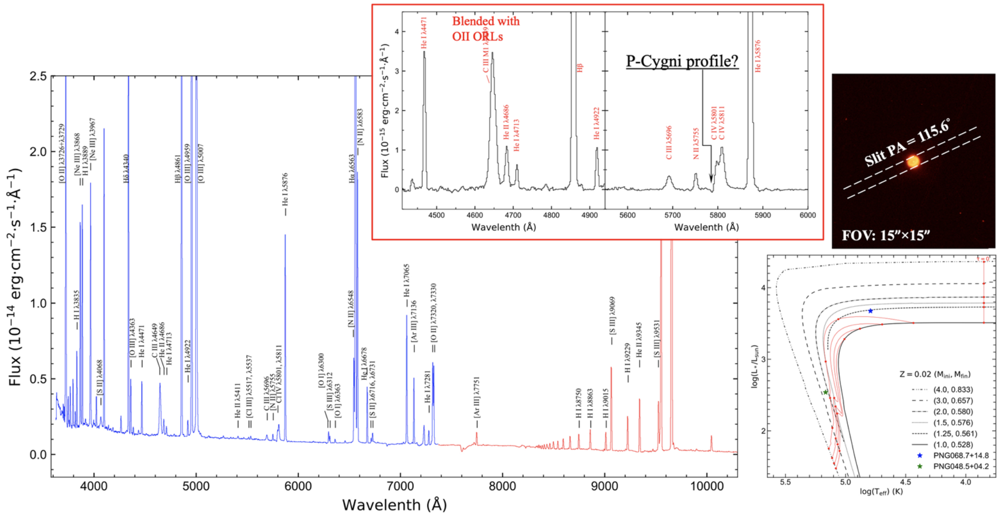

Figure 2. *Left*: GTC OSIRIS long-slit spectrum of Galactic planetary nebula PN G068.7+14.8; blue and red represent the R1000B and R1000R grisms, respectively. *Right-top*: *HST* WFC3 F502N narrowband image of PN G068.7+14.8 in the [O III] λ5007 emission line, adopted from Stanghellini, Shaw & Villaver (2016); the GTC long slit (white-dashed lines) with 1-arcsec width is overlaid. *Right-bottom*: Central star position of PN G068.7+14.8 (blue star) in H-R diagram, where model tracks of the H-burning post-AGB sequences calculated by Miller Bertolami (2016) at $Z = 0.02$ are overplotted, different line types representing different initial and final masses. The red curves are the isochrones for evolutionary ages ($\tau = 0$, 5000, 10,000, 15,000, and 20,000 years) since the beginning of post-AGB defined at $\log T_{\rm eff} = 3.85$. The central star position of another Galactic compact nebula PN G048.5+04.2 (green star) is also presented for purpose of comparison of a different evolutionary status from that of PN G068.7+14.8. *Top-inset*: Zoom-in of the GTC spectrum showing the C III and C IV lines possibly emitted from the central star, with a likely P-Cygni profile marked (Huang & Fang, in preparation).

our PNe using the multi-wavelength spectra. Cloudy photoionization models, with an aid of the *HST* optical images (Stanghellini, Shaw & Villaver 2016), will be developed based on the UV-optical-IR spectra, to derive the central star masses of our sample PNe and consequently, the main-sequence masses/ages. We will compare the chemical abundances with predictions from the stellar evolution models – in particular the AGB nucleosynthesis models (e.g. Karakas & Lugaro 2016), and correlate them with the dust chemistry, metallicity and central star masses.

Given the distribution (Galactic l and b, distance) of our sample in the Galaxy, it is suitable to explore the nebular and stellar properties across the Galactic disk. Our Northern sample is complemented by the previous observations of the Southern objects (using the 4.1-m SOAR telescope) and other published spectroscopy. With the available *Gaia* distances, we will set strong constraints on the Galactic evolutionary models through the analysis of chemical (oxygen and other α-elements) and population gradients using these compact PNe.

3. Spectroscopic Survey of the PNe in M31 halo

Since 2012, large-aperture (8–10 m class) optical telescopes have been used to obtain the spectra of PNe in M31, mostly in M31's outer disk (Kwitter et al. 2012; Balick et al. 2013; Corradi et al. 2015), and all have oxygen abundances close to the solar level. Spectroscopic analysis of the outer-halo PNe in M31 were extremely scarce. Our first attempt of optical spectroscopy of bright PNe in the outer halo in the Northern Spur

https://doi.org/10.1017/S1743921324000486 Published online by Cambridge University Press

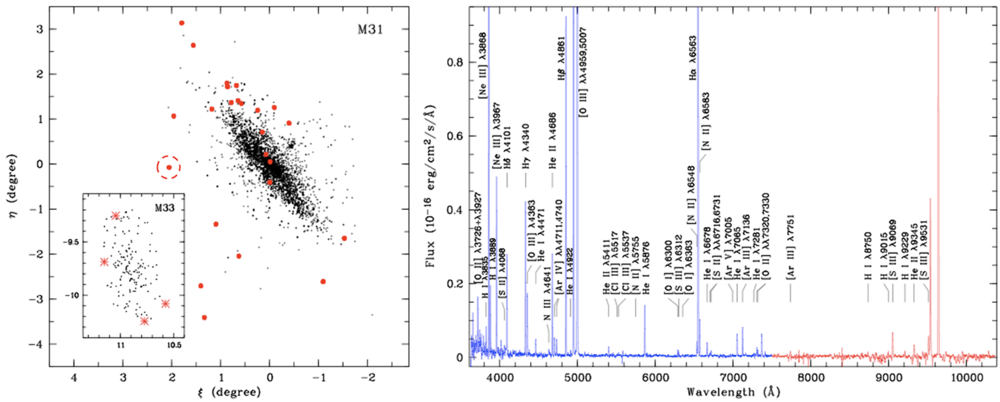

Figure 3. *Left*: Distribution of PNe in M31+M33. The PNe targeted by our GTC observations (Fang et al. 2013, 2015, 2018, and several unpublished objects) are highlighted in red-filled circles and red asterisks. The inset shows the PNe in M33 in M31-centred coordinates. *Right*: GTC OSIRIS long-slit spectrum of a halo PN in M31 (marked by a red-dashed circle in the *left* panel) obtained with the R1000B (blue) and R1000R (red) grisms, with emission lines labeled.

substructure) of M31 was carried out using the 5.1-m Hale telescope, only with limited data quality, although our analysis revealed metal-rich nature of the halo objects (Fang et al. 2013). Since 2014, we continued this effort using the 10.4-m GTC in La Palma. So far, over 100 hr observations have been completed at the GTC for ∼30 PNe in M31's halo (Figure 3), mostly with excellent spectral quality (e.g. Figure 3-*right*). Our halo samples kinematically deviate from the disk population, and were carefully selected so that they are located in different halo substructures, covering a vast spatial extension (Figure 3-*left*). The instrument setup (spectrograph, grisms, slit width and observing mode) and procedure of data reduction are the same as introduced in Section 2.

All the outer-halo PNe of M31 we have published so far also have oxygen abundances close to the Sun, [O/H]$\gtrsim -0.4$ with modest scatter (Fang et al. 2013, 2015, 2018, see also Figure 4), and probably all evolved from low-mass ($<2\,M_{\odot}$) stars mostly with ages of ∼2–5 Gyr. Our halo sample cannot be distinguished from the disk population in metallicity or the main-sequence mass/age (Fang et al. 2018), which is in stark contrast with the underlying, smooth, metal-poor halo of M31 (Figure 4). We conjecture that these halo PNe might have originally formed from metal-rich gas in M31 disk but were displaced to the halo regions and gained their current stream/substructure kinematics as a result of M31's interaction with its satellite(s). This astrophysical picture, although highly speculative, agrees with our present-day knowledge that M31's extended halo evolved from complex galactic mergers and interactions. Further investigation using a combined sample in M31+M33 is underway (Fang et al. 2023b, in preparation).

Photoionization models will be constructed for the halo/substructure PNe in M31 to derive their main-sequence masses ($M_{\rm ini}$). We will then derive the He/H and N/O abundance ratios versus $M_{\rm ini}$ relations for the combined sample of the halo/substructure PNe in M31 together with the Galactic compact PNe observed using GTC (see Section 2). These abundance-mass relations will be used to constrain the AGB models. The surface contents of helium and nitrogen are expected to increase as a consequence of the second dredge up and HBB that occur in intermediate-mass AGB stars with $M_{\rm ini}\gtrsim$3–5 $M_{\odot}$(e.g. Karakas & Lugaro 2016). However, previous spectroscopic analysis of M31 and Galactic PNe indicates that HBB might actually occur at $<3\,M_{\odot}$. Our new observations will be used to carefully assess this (Fang et al. 2023b, in preparation).

https://doi.org/10.1017/S1743921324000486 Published online by Cambridge University Press

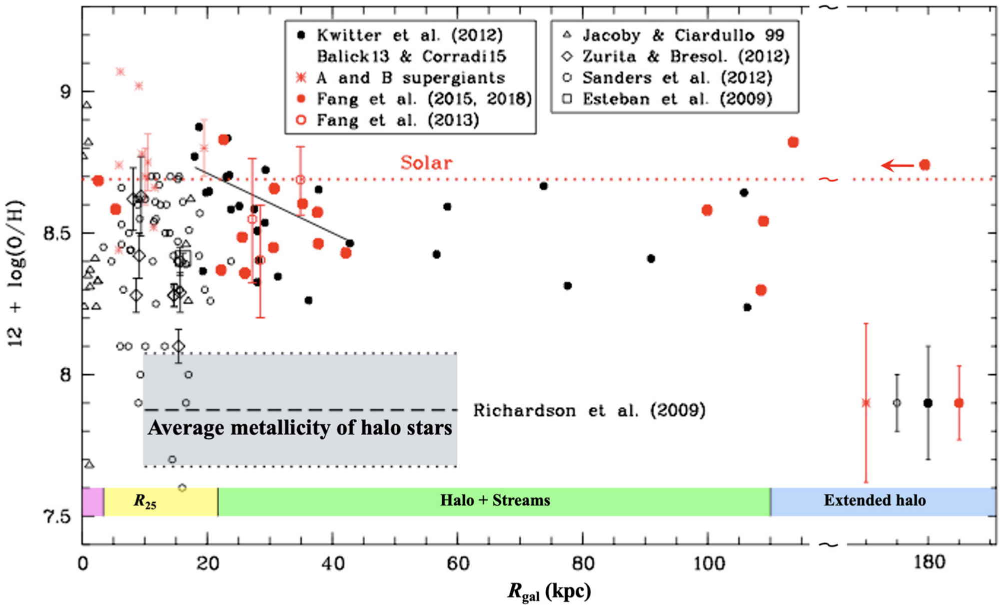

Figure 4. Radial distribution of oxygen abundances in M31 (figure adopted from Fang et al. 2018). The M31 halo PNe previously targeted by our GTC observations are red-filled circles (see Figure 3-*left*). The M31 outer-disk PNe (observed by Kwitter et al. 2012, Balick et al. 2013, and Corradi et al. 2015) are black dots. Other literature samples of PNe, H II regions and supergiants in M31 are over-plotted (see legend). The black-solid straight line is a linear fit to the disk PNe between 20 and 40 kpc (Kwitter et al. 2012). The red-dotted line marks the solar value. The horizontal black-dashed and dotted lines represent the mean metallicity and dispersion (also grey-shaded) of halo stars between 10 and 60 kpc (Richardson et al. 2009).

References

Balick B., Kwitter K. B., Corradi R. L. M., & Henry R. B. C., 2013, *ApJ*, 774, 3, DOI:10.1088/0004-637X/774/1/3

Corradi R. L. M., Kwitter K. B., Balick B., et al., 2015, *ApJ*, 807, 181, DOI:10.1088/0004-637X/807/2/181

Dufour R. J., Kwitter K. B., Shaw R. A., et al., 2015, *ApJ*, 803, 23, DOI:10.1088/0004-637X/803/1/23

Gerhard O., Arnaboldi M., Freeman K. C., et al., 2005, *ApJL*, 621, L93, DOI:10.1086/429221

Gerhard O., Arnaboldi M., Freeman K. C., et al., 2007, *A&A*, 468, 815, DOI: 10.1051/0004-6361:20066484

Fang X., Zhang Y., Garía-Benito R., Liu X.-W., & Yuan H.-B., 2013, *ApJ*, 774, 138, DOI:10.1088/0004-637X/774/2/138

Fang X., García-Benito R., Guerrero M. A., et al., 2015, *ApJ*, 815, 69, DOI:10.1088/0004-637X/815/1/69

Fang X., García-Benito R., Guerrero M. A., et al., 2018, *ApJ*, 853, 50, DOI:10.3847/1538-4357/aaa1e5

Ferland G. J., Chatzikos M., Guzmán F., et al., 2017, *RMxAA*, 53, 385, DOI:10.48550/arXiv.1705.10877

Ferland G. J., Korista K. T., Verner D. A., et al., 1998, *PASP*, 110, 761, DOI:10.1086/316190

Hammer F., Yang Y. B., Wang J. L., et al., 2018, *MNRAS*, 475, 2754, DOI:10.1093/mnras/stx3343

Henry R. B. C., Stephenson B. G., Miller Bertolami M. M., Kwitter K. B., & Balick B., 2018, *MNRAS*, 473, 241, DOI:10.1093/mnras/stx2286

Herwig F., 2005, *ARA&A*, 43, 435, DOI:10.1146/annurev.astro.43.072103.150600

Ibata R. A., Irwin M. J., Lewis G., et al., 2001, *Nature*, 412, 49, DOI:10.1038/35083506
Karakas A. I., & Lugaro M., 2016, *ApJ* 825, 26, DOI:10.3847/0004-637X/825/1/26
Kingsburgh R. L., & Barlow M. J., 1994, *MNRAS*, 271, 257, DOI:10.1093/mnras/271.2.257
Kwitter K. B., Lehman E. M. M., Balick B., & Henry R. B. B., 2012, *ApJ*, 753, 12, DOI:10.1088/0004-637X/753/1/12
Longobardi A., Arnaboldi M., Gerhard O., et al., 2018, *A&A*, 620, A111, DOI:10.1051/0004-6361/201832729
McConnachie A. W., Irwin M. J., Ferguson A. M. N., et al., 2005, *MNRAS*, 356, 979, DOI:10.1111/j.1365-2966.2004.08514.x
McConnachie A. W., Irwin M. J., Ibata R. A., et al., 2009, *Nature*, 461, 66, DOI:10.1038/nature08327
Merrett H. R., Kuijken K., Merrifield M. R., et al., 2003, *MNRAS*, 346, L62, DOI:10.1111/j.1365-2966.2003.07367.x
Milingo J. B., Kwitter K. B., Henry R. B. C., & Souza S. P., 2010, *ApJ*, 711, 619, DOI:10.1088/0004-637X/711/2/619
Miller Bertolami M. M., 2016, *A&A*, 588, A25, DOI:10.1051/0004-6361/201526577
Osterbrock D. E., & Ferland G. J., 2006, Astrophysics of Gaseous Nebulae and Active Galactic Nuclei (Sausalito, CA: Univ. Science Books)
Richardson J. C., Ferguson A. M. N., Mackey A. C., et al., 2009, *MNRAS*, 396, 1842, DOI:10.1111/j.1365-2966.2009.14788.x
Stanghellini L., García-Hernández D. A., García-Lario P., et al., 2012, *ApJ*, 753, 172, DOI:10.1088/0004-637X/753/2/172
Stanghellini L., & Haywood M., 2010, *ApJ*, 714, 1096, DOI:10.1088/0004-637X/714/2/1096
Stanghellini L., Shaw R. A., & Villaver E., 2016, *ApJ*, 830, 33, DOI:10.3847/0004-637X/830/1/33